Mineralogical Magazine, February 2015, Vol. 79(1), pp. 191–203

Structural intergrowth of merlinoite/phillipsite and its temperature-dependent dehydration behaviour: a single-crystal X-ray study

ROSA MICAELA DANISI[1,*], THOMAS ARMBRUSTER[1] AND MARIKO NAGASHIMA[2]

[1] Mineralogical Crystallography, Institute of Geological Sciences, University of Bern, Freiestrasse 3, CH-3012 Bern, Switzerland

[2] Graduate School of Science and Engineering, Yamaguchi University, Yoshida 1677-1, Yamaguchi 753-8512, Japan

[*Received 20 February 2014; Accepted 25 July 2014; Associate Editor: A. Christy*]

ABSTRACT

Supposed 'merlinoite' crystals from Monte Somma, Vesuvius (Italy) and Fosso Attici, north of Rome (Italy) represent highly twinned coherent intergrowths between merlinoite and phillipsite on a submicroscopic level. The MER (*Immm*, $a \approx 14.1$, $b \approx 14.2$, $c \approx 9.9$ Å) and PHI ($P2_1/m$, $a \approx 9.9$, $b \approx 14.3$, $c \approx 8.7$ Å, $\beta = 124.8°$) frameworks of similar composition are assembled from identical tetrahedral units, though with a different connectivity. Coherent intergrowth and twinning of the two frameworks lead to $P4_2/mnm$ pseudosymmetry, which is diagnostic of the intergrowth. Under ambient conditions merlinoite has *Immm* symmetry or *I*4/*mmm* if twinned. A low-symmetry model of space group $P12_1/m1$ ($a \approx 14.2$, $b \approx 14.2$, $c \approx 10$ Å, $\beta = 90°$) allows structure refinement and quantification of the two frameworks.

Upon *in situ* dehydration to 250ºC the evolution of the unit-cell volume of the Monte Somma merlinoite/phillipsite intergrowth displays an intermediate trend between previously studied pure merlinoite from the Khibiny massif (Russia) and Ba-rich phillipsite.

The Monte Somma crystal studied by temperature-dependent single-crystal X-ray diffraction methods also contained a subordinate chabazite inclusion with no coherent structural relationship to the merlinoite/phillipsite framework. Thus, the modification of the chabazite framework on dehydration could also be studied.

KEYWORDS: zeolite, merlinoite, phillipsite, chabazite, crystal structure, dehydration, intergrowth.

Introduction

MERLINOITE, framework code MER, is a rare natural zeolite (Passaglia *et al*., 1977) with a framework assembled from four- and eight-membered rings of tetrahedra (Galli *et al*., 1979). Merlinoite of $K_5Ca_2[Al_9Si_{23}O_{64}]\cdot 24H_2O$ composition was first found in cavities of alkaline basaltic lava in the Cupaello quarry near Santa Rufina, Rieti, Italy (Passaglia *et al*., 1977). The crystal structure, space group *Immm* (No.71), $a = 14.116(7)$, $b = 14.229(6)$, $c = 9.946(6)$ Å (Galli *et al*., 1979) is actually pseudo-tetragonal. The MER framework possesses tetragonal topology with maximum space-group symmetry *I*4/*mmm*. In merlinoite, the framework has a statistical (Al, Si) distribution but the extra-framework cation and H_2O distribution combined with the cation bonding to the framework reduces the symmetry to orthorhombic (Galli *et al*., 1979). Merlinoite has a synthetic counterpart named zeolite W (Sherman, 1977; Bieniok *et al*., 1996; Skofteland

* E-mail: rosamicaela.danisi@libero.it
DOI: 10.1180/minmag.2015.079.1.15

et al., 2001), also of orthorhombic symmetry (space group *Immm*).

In a previous study (Pakhomova *et al*., 2014), the dehydration of merlinoite, $NaK_{11}[Al_{12}Si_{20}O_{64}]\cdot 15H_2O$, from Khibiny massif (Russia) was investigated by single-crystal X-ray diffraction (XRD) methods and the evolution of the structural distortion upon dehydration determined. Surprisingly, the type of structural distortion of partially and fully dehydrated samples was different from a synthetic sample of similar $K_{11.5}[Al_{11.5}Si_{20.5}O_{64}]\cdot 15H_2O$ composition, which Skofteland *et al.* (2001) used to study dehydration by Rietveld refinement of powder XRD. In the refinement by Skofteland *et al.* (2001), the eight-membered rings perpendicular to the pseudo-tetragonal direction adopt an elliptical cross-section, whereas in the Pakhomova *et al*. (2014) study the corresponding cross-sections show quadratic apertures due to an overlay of adjacent elliptical rings rotated by 90º relative to each other. These differences in dehydration behaviour motivated us to select additional merlinoite crystals of different composition, to explore the reasons for the distinct differences in framework distortion upon loss of water. An overview of the few merlinoite occurrences was provided by Pakhomova *et al*. (2014). Merlinoite from the type locality appeared to be too finely crystalline, and thus not suited for a high-temperature single-crystal X-ray study. Only samples from Monte Somma, Vesuvius (Italy) and Fosso Attici, north of Rome, Italy (Della Ventura *et al*., 1993) fulfilled crystal-size requirements for a dehydration study. However, as shown in this present study, the newly investigated samples are not pure merlinoite but represent a coherent intergrowth between merlinoite and phillipsite.

Experimental

Three different samples of merlinoite crystals were investigated, two from Monte Somma (Vesuvius) and one from Fosso Attici north of Rome (courtesy of Giancarlo Della Ventura). The three samples are: sample A (Armbruster collection), sample B (Natural History Museum Bern, NMBE 42529) and sample C (the crystal from G. Della Ventura). Merlinoite from Monte Somma forms sprays of prismatic crystals within lava cavities (Fig. 1), which resemble those described by Russo and Preite (2011). The chemical composition of the Fosso Attici sample has been reported as $K_{5.02}Na_{0.66}Ba_{0.32}Sr_{0.07}Fe_{0.05}Ca_{1.60}Mn_{0.08}Mg_{0.03}(Al_{10.79}Si_{21.21})O_{64}\cdot 20.1H_2O$ (Della Ventura *et al*., 1993).

Samples A and B from Monte Somma were analysed using a JEOL JXA-8230 electron microprobe installed at Yamaguchi University; operating conditions were 15 kV accelerating voltage, 2 nA probe current and 10 μm beam diameter. Before and after the measurements, standard materials such as albite and K-feldspar were analysed to check the accuracy of the results. The following elements were measured using standard materials for calibration: Si and Ca (wollastonite), Ti (rutile), Al (corundum or albite), Cr (eskolaite), V ($Ca_3(VO_4)_2$), Fe (hematite), Mn (MnO), Mg (periclase), Na (albite), K (K-feldspar), Sr and Ba ($SrBaNb_4O_{12}$), Ni (NiO), P ($KTiOPO_4$), F (fluorite) and Cl (halite).

Three different types of crystal fragments from the Monte Somma samples were investigated by single-crystal X-ray methods: (1) tip of the crystal; (2) base of the crystal; and (3) whole crystal. Different crystal portions were selected to analyse the distribution of merlinoite–phillipsite domains. The crystal structures of all samples were determined at room temperature. In addition, for a crystal from Monte Somma (sample B, whole crystal), high-temperature experiments with *in situ* XRD were performed. The crystal studied, with dimensions 0.30 mm × 0.25 mm × 0.20 mm, was squeezed into a conical quartz-glass capillary with an open diameter of 0.2 mm. The sample was heated in 25ºC increments to 250ºC using an in-house designed nitrogen

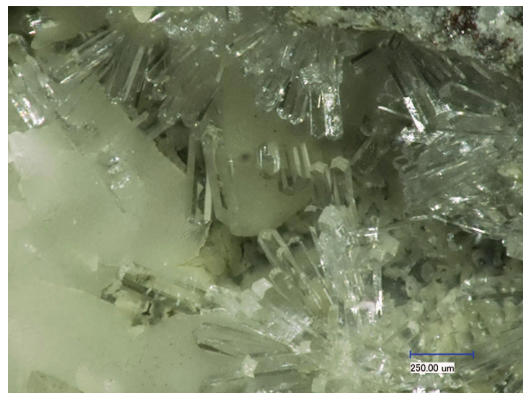

FIG. 1. 'Merlinoite' sample B from Monte Somma, Vesuvius (Museum of Natural History Bern, NMBE 42529).

https://doi.org/10.1180/minmag.2015.079.1.15 Published online by Cambridge University Press

stream-heater (University of Bern). Before high-temperature data collection, the crystal was kept at a given temperature for 30 min. Data collection at each temperature took ~10 h. At each temperature more than a hemisphere of three-dimensional data was collected by means of a Bruker APEX II diffractometer equipped with CCD detector using Mo$K\alpha$ (0.71073 Å) radiation, generator voltage and current of 50 kV and 30 mA, respectively, a crystal-to-detector distance of 50 mm and frame widths of 0.5º in ω and φ. Exposure time per frame was 10 s for data collection. Data-collection parameters and refinement parameters are given in Tables 1 and 2. The crystal from Fosso Attici produced a blurred diffraction pattern but all the merlinoite samples from Monte Somma displayed sharp diffraction spots. Systematic extinctions indicated that the symmetry was $P4_2/mnm$ and not $Immm$ or $I4/mmm$, that had been expected for merlinoite. Structure solution by direct methods and subsequent refinement converged at $R1$ values between

TABLE 1. Parameters for X-ray data collection and crystal-structure refinement of merlinoite/phillipsite intergrowth.

Crystal data	Merlinoite/Phillipsite (RT)	Merlinoite/Phillipsite (250ºC)
Unit-cell dimensions (Å)	a = 14.2017(7) b = 14.2017(7) c = 9.9692(5) β = 90.000(5)	a = 13.4935(3) b = 13.4935(3) c = 9.8112(2) β = 90.000(5)
Volume (Å^3)	2010.67(17)	1786.37(7)
Space group	$P12_1/m1$ (No. 11)	$P12_1/m1$ (No. 11)
Z	1	1
Chemical formula	$CaK_7[Al_9Si_{23}O_{64}]\cdot xH_2O$	$CaK_7[Al_9Si_{23}O_{64}]\cdot xH_2O$
Intensity measurement		
Crystal shape	Prismatic	Prismatic
Crystal size (mm)	0.30 × 0.25 × 0.20	0.30 × 0.25 × 0.20
Diffractometer	APEX II SMART	APEX II SMART
X-ray radiation	Mo$K\alpha$ λ = 0.71073 Å	Mo$K\alpha$ λ = 0.71073 Å
X-ray power	50 kV, 30 mA	50 kV, 30 mA
Monochromator	Graphite	Graphite
Temperature	296 K	523 K
Time per frame (s)	10	10
Max. θ (º)	34.745	28.656
Index ranges	$-21 \leqslant h \leqslant 20$ $-22 \leqslant k \leqslant 22$ $-15 \leqslant l \leqslant 15$	$-18 \leqslant h \leqslant 18$ $-18 \leqslant k \leqslant 18$ $-13 \leqslant l \leqslant 13$
No. of measured reflections	42,244	62,182
No. of unique reflections	8698	4788
No. of observed reflections ($I > 2\sigma(I)$)	6221	3813
Refinement of the structure		
No. of parameters used in refinement	353	333
R_{int}	0.0421	0.0559
R_σ	0.0446	0.0285
$R1$, $I > 2\sigma(I)$	0.1033	0.1409
$R1$, all data	0.1342	0.1690
w$R2$ (on F^2)	0.2574	0.3687
Gof	2.708	4.988
$\Delta\rho_{min}$ ($-$e / Å^3)	−4.04 close to Q22	−1.57 close to Si6M
$\Delta\rho_{max}$ (e / Å^3)	1.24 close to O5	1.44 close to Q16

https://doi.org/10.1180/minmag.2015.079.1.15 Published online by Cambridge University Press

TABLE 2. Parameters for X-ray data collection and crystal-structure refinement of chabazite.

Crystal data	Chabazite (50ºC)	Chabazite (125ºC)	Chabazite (150ºC)	Chabazite (250ºC)
Unit-cell dimensions (Å)	a = 13.798(2) b = 13.798(2) c = 14.862(3) γ = 120	a = 13.6950(19) b = 13.6950(19) c = 14.993(3) γ = 120	a = 13.5468(19) b = 13.5468(19) c = 15.306(3) γ = 120	a = 13.4275(19) b = 13.4275(19) c = 15.510(3) γ = 120
Volume (Å^3)	2450.5(9)	2435.3(8)	2432.5(8)	2421.7(8)
Space group	$R\bar{3}m$ (No. 166)	$R\bar{3}m$ (No. 166)	$R\bar{3}m$ (No. 166)	$R\bar{3}m$ (No. 166)
Z	6	6	6	6
Chemical formula	$Ca[Al_2Si_4O_{12}]$	$Ca[Al_2Si_4O_{12}]$	$Ca[Al_2Si_4O_{12}]$	$Ca[Al_2Si_4O_{12}]$
Intensity measurement				
Crystal shape	Prismatic	Prismatic	Prismatic	Prismatic
Crystal size (mm)	0.30 × 0.25 × 0.20	0.30 × 0.25 × 0.20	0.30 × 0.25 × 0.20	0.30 × 0.25 × 0.20
Diffractometer	APEX II SMART	APEX II SMART	APEX II SMART	APEX II SMART
X-ray radiation	Mo$K\alpha$ λ = 0.71073 Å	Mo$K\alpha$ λ = 0.71073 Å	Mo$K\alpha$ λ = 0.71073 Å	Mo$K\alpha$ λ = 0.71073 Å
X-ray power	50 kV, 30 mA	50 kV, 30 mA	50 kV, 30 mA	50 kV, 30 mA
Monochromator	Graphite	Graphite	Graphite	Graphite
Temperature	323 K	398 K	423 K	523 K
Time per frame (s)	10	10	10	10
Max. θ (º)	34.775	29.708	28.528	28.656
Index ranges	$-22 \leqslant h \leqslant 22$ $-22 \leqslant k \leqslant 22$ $-23 \leqslant l \leqslant 23$	$-19 \leqslant h \leqslant 19$ $-19 \leqslant k \leqslant 19$ $-20 \leqslant l \leqslant 20$	$-18 \leqslant h \leqslant 18$ $-18 \leqslant k \leqslant 20$ $-20 \leqslant l \leqslant 20$	$-18 \leqslant h \leqslant 18$ $-18 \leqslant k \leqslant 18$ $-20 \leqslant l \leqslant 20$
No. of measured reflections	35,123	34,669	32,483	32,393
No. of unique reflections	1307	861	782	787
No. of observed reflections (I> 2σ(I))	645	486	435	429
Refinement of the structure				
No. of parameters used in refinement	38	36	39	44
R_{int}	0.3444	0.3655	0.3922	0.6641
R_σ	0.1178	0.0779	0.0810	0.1211
$R1$, $I > 2\sigma(I)$	0.1562	0.1716	0.1460	0.1892
$R1$, all data	0.2580	0.2453	0.2056	0.2700
w$R2$ (on F^2)	0.3775	0.3931	0.3877	0.4209
Gof	1.882	2.240	2.177	2.243
$\Delta\rho_{min}$ (−e / Å^3)	−1.24 close to K1	−1.33 close to K1	−0.76 close to SI1	−1.64 close to K3
$\Delta\rho_{max}$ (e / Å^3)	4.22 close to K1	3.36 close to O1	2.61 close to O1	2.73 close to O1

20 and 30%, indicating a merlinoite-like structure. If the weak reflections responsible for the primitive Bravais-type were rejected and refinements were conducted in *Immm* or *I*4/*mmm* symmetry, corresponding *R*1 values dropped slightly below 10%. Based on remarks in the literature (Galli *et al*., 1979; Sato and Gottardi, 1982; Tschernich, 1992; Russo and Preite, 2011), we suspected twinning and coherent intergrowth of merlinoite and phillipsite. Thus, the composite structure required a special refinement strategy, explained in the results below. Crystallographic information files (cif) have been deposited with the Principal Editor of *Mineralogical Magazine* and are available from www.minersoc.org/pages/e_journals/dep_mat_ mm.html.

Results

Under high-vacuum conditions during electron-microprobe investigation, the zeolites partly dehydrated and the originally polished surface became cracked and uneven. The low analytical totals obtained were consistent with a water content of 7–14 H_2O per formula unit. The lowest totals and hence possibly greatest water content were associated with high Ca content. For sample A crystal 4 (Fig. 2) from Monte Somma (22 point measurements, Table 3), compositions with the largest (A04–04) and the smallest (A04–02) Ca content were: $Ca_{2.03}Na_{0.31}K_{5.36}[Al_{9.82}Si_{22.18}O_{64}]$ and $Ca_{1.10}Na_{0.41}K_{6.97}[Al_{9.32}Si_{22.68}O_{64}]$, respectively. The average composition of 89 analytical points, collected on four crystals, was $Ca_{1.23}Na_{0.43}K_{6.64}[Al_{9.46}Si_{22.54}O_{64}]$. Approximately 45 point analyses were collected on four crystals of sample B (Table 3) and the largest and smallest Ca contents were represented by the compositions $Ca_{1.36}Na_{0.43}K_{6.37}[Al_{9.47}Si_{22.53}O_{64}]$ and $Ca_{0.19}Na_{0.28}K_{8.41}[Al_{9.16}Si_{22.84}O_{64}]$, respectively, with an average composition of $Ca_{0.48}Na_{0.51}K_{7.72}[Al_{9.09}Si_{22.91}O_{64}]$. Distinct merlinoite and phillipsite domains could not be distinguished, either optically using crossed polarizers, or by element mapping (Fig. 3). All crystals showed zonal variation in the Ca:K ratio on very fine scale (Figs 2 and 3). The bright features parallel to the *c* axis seen under crossed polars (Figs 2 and 4) were interpreted as twin boundaries of domains related by 90º rotation around *c*. All crystals examined displayed some undulatory extinction associated with patchy domains or lamellar microstructures (Figs 2 and 4).

The merlinoite unit cell and the doubled phillipsite unit cell (V ~2000 Å^3), as shown in Fig. 5, each consist of 32 tetrahedral sites (Galli *et al*., 1979). The topology of the two structures is

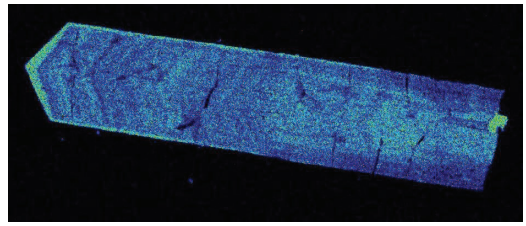

FIG. 3. Map of Ca concentration in Sample A; light blue = high Ca. Crystal cross-section ≈100 μm.

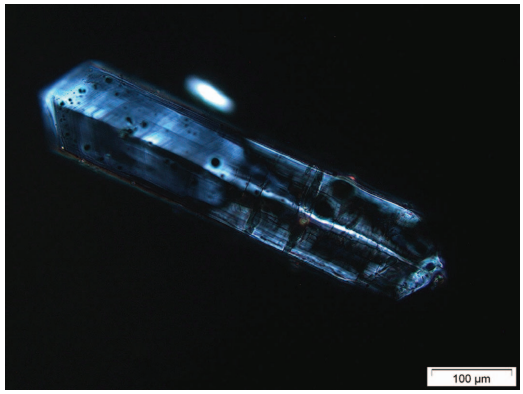

FIG. 2. Monte Somma Sample A photographed with crossed polarizers.

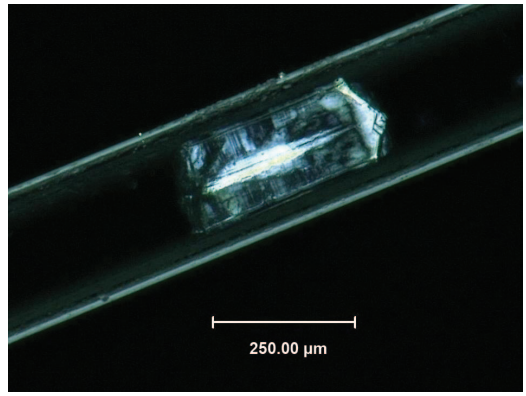

FIG. 4. Fosso Attici merlinoite/phillipsite prepared in a glass capillary and photographed under crossed polarizers.

https://doi.org/10.1180/minmag.2015.079.1.15 Published online by Cambridge University Press

distinguished by a different arrangement of eight (of 32 = ¼ of the total) tetrahedral *T* sites. In the space group $P4_2/mnm$, the multiplicity of a general position is 16, leading to only two symmetrically distinct *T* sites. Thus, $P4_2/mnm$ symmetry is not compatible with an ordered intergrowth of a phillipsite-like structure. A cyclic orthorhombic *Pnnm* twin with a 90º rotation around the *c* axis would also be consistent with the observed systematic absences, and would allow four symmetrically distinct tetrahedral sites. However, no single *T* site would split into two subsites, one characteristic of merlinoite and the other of phillipsite. For this reason the symmetry was further decreased to a monoclinic twin (90º rotation around *c*) and refinement in space group $P12_1/m1$ with a merlinoite-like unit cell ($a \approx 14.2$, $b \approx 14.2$, $c \approx 10$ Å, $\beta = 90º$, Fig. 5), which allowed splitting of two of the eight tetrahedral sites into merlinoite-like and phillipsite-like subsites. The intensity data were integrated and corrected for absorption and Lorentz polarization using the *SAINT* software package (Bruker, 1999). Structure solution and refinement were carried out with *SHELXS* and *SHELXL* (Sheldrick, 2008) using neutral-atom scattering factors. Two *T* and eight O sites were split into merlinoite- and phillipsite-like positions. The occupancies of split subsites were constrained to a common value and refined. Refinements in space group $P12_1/m1$, allowing for anisotropic atomic displacement parameters and variable occupancies of extra-framework positions, converged to *R*1 of ~10%. Owing to the overlay of two different frameworks combined with the strong similarity of the channel system, it was not possible to assign extra-framework species to either one of the zeolite structures.

The Monte Somma crystal used for *in situ* dehydration experiments showed not only diffraction corresponding to the merlinoite-phillipsite intergrowth, but also sharp reflections corresponding to a quite different structure. The additional pattern, comprising a few thousand reflections, had $R\bar{3}m$ symmetry and was identified as characteristic of chabazite. Thus, the dehydration behaviour of the small chabazite inclusion could also be tracked. Some of the chabazite reflections were overlapping with some of those of the merlinoite/phillipsite intergrowth, explaining the very poor internal *R* values (Table 2).

Discussion

Coherent merlinoite/phillipsite intergrowth

Neither optical micrographs taken with crossed polarizers (Figs. 2 and 4) nor element distributions mapped by electron microprobe provide any information about the size of different domains. Thus the intergrowth is assumed to occur at a submicroscopic level. Samples from Monte Somma converged to a merlinoite/phillipsite ratio of ~1/1, varying between 0.6/0.4 and 0.4/0.6 in the three crystals studied. The sample from Fosso Attici consisted of 67% merlinoite and 33% phillipsite. Reconstructions of *h*0*l* reciprocal space layers showed additional weak reflections in the Fosso Attici pattern obeying a strict orientation relation to the main merlinoite/

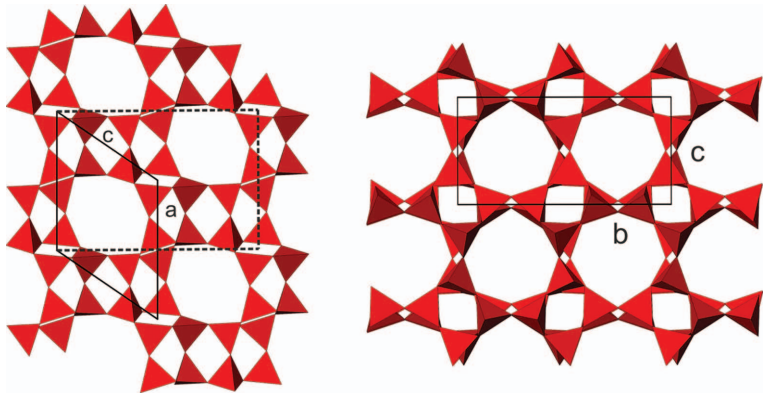

FIG. 5. Tetrahedral framework of phillipsite (Gatta *et al*., 2009). (Left) Projection along the *b* axis. (Right) Projection along *a*. Solid outlines: conventional phillipsite unit cell $a = 9.85$, $b = 14.25$, $c = 8.64$ Å, $\beta = 124.3º$; dashed outline: merlinoite-like cell setting.

https://doi.org/10.1180/minmag.2015.079.1.15 Published online by Cambridge University Press

phillipsite lattice. These reflections could not be interpreted.

As noted above, the merlinoite and phillipsite frameworks are distinguished by the differing orientation and placement of only ¼ of the tetrahedra. Different views of the two structures are shown in Fig. 6. Tetrahedra highlighted in yellow are different; those shown in red are common to both frameworks. The yellow tetrahedral dimers in Fig. 6*a* are shifted by *b*/2 from merlinoite to phillipsite. Projections along the *b* axis (Fig. 6*b*) appear very similar for merlinoite and phillipsite but due to the *b*/2 shift of the yellow dimers, the connectivity to the adjacent red tetrahedra is different. The difference between the two structures is most striking in projections along the *a* axis (Fig. 6*c*). In phillipsite projected along *a*, the *b*/2 shifted four-membered rings of tetrahedra (yellow) plug the eight-membered rings. In a corresponding projection for the merlinoite domain, yellow four-membered rings are overlain by red rings at a different *x* level (Fig. 6*c*).

As shown by a comparison of Figs 5 and 6, there are minor distortional differences between

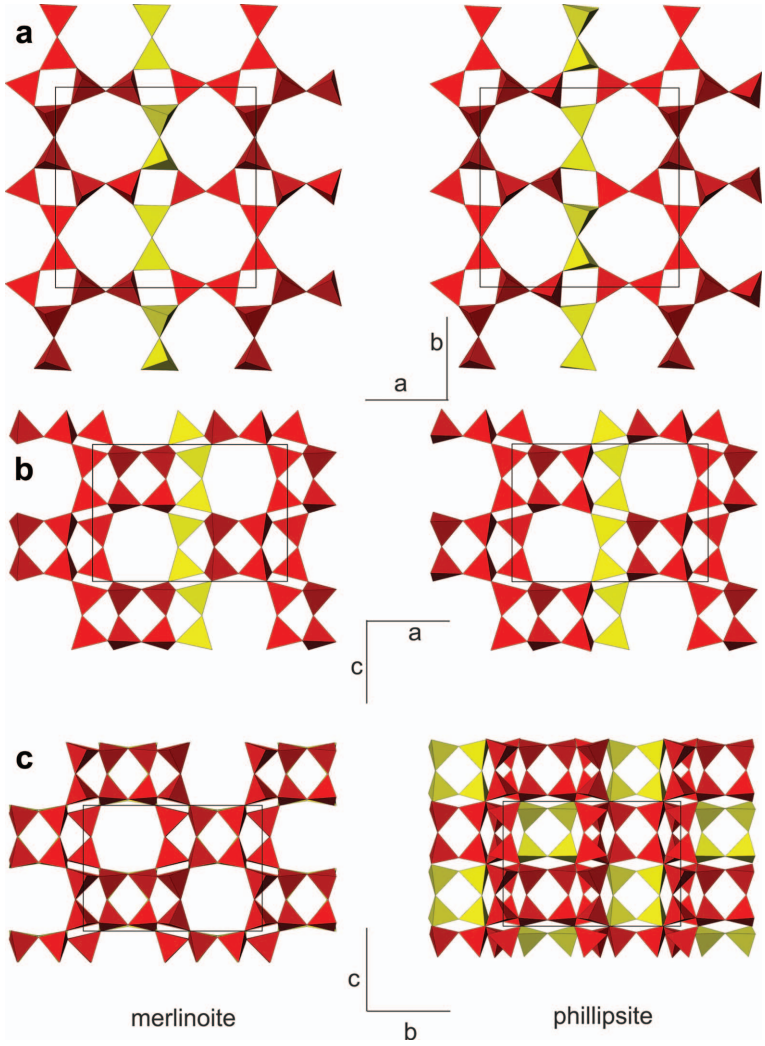

FIG. 6. Refined merlinoite (left) framework and corresponding view of phillipsite (right), viewed (*a*) down the *c* axis of merlinoite, (*b*) down the *b* axis and (*c*) down the *a* axis. The yellow colour highlights the tetrahedra that are oriented and connected differently in the two structures.

https://doi.org/10.1180/minmag.2015.079.1.15 Published online by Cambridge University Press

TABLE 3. Results of electron microprobe analyses from Monte Somma samples (A and B).

	A04−04 high Ca	A04−02 low Ca	Average A 89 points	B03−05 high Ca	B03−21 low Ca	Average B 45 points
SiO_2	54.09	57.04	55.63	55.97	56.82	56.81
TiO_2	0.04	0.04	0.04	0.04	0.00	0.04
Al_2O_3	20.30	19.88	19.82	19.97	19.35	19.12
Cr_2O_3	0.00	0.00	0.08	0.00	0.00	0.06
V_2O_3	0.00	0.02	0.03	0.03	0.00	0.03
Fe_2O_3	0.00	0.00	0.05	0.00	0.00	0.07
MnO	0.00	0.14	0.06	0.03	0.14	0.05
MgO	0.06	0.03	0.04	0.11	0.01	0.07
CaO	4.61	2.37	2.83	3.15	0.45	1.11
SrO	0.00	0.00	0.03	0.00	0.00	0.05
BaO	0.05	0.00	0.11	0.00	0.05	0.11
Na_2O	0.39	0.54	0.55	0.55	0.37	0.65
K_2O	10.24	13.75	12.84	12.41	16.40	15.01
NiO	0.00	0.21	0.04	0.05	0.00	0.04
P_2O_5	0.00	0.06	0.03	0.00	0.01	0.02
F	0.24	0.24	0.09	0.00	0.00	0.09
Cl	0.03	0.04	0.01	0.00	0.00	0.01
Total	90.04	94.33	92.27	92.32	93.59	93.34
H_2O	9.96	5.67	7.73	7.68	6.41	6.66
Si+Al =	32	32	32	32	32	32
Si	22.18	22.68	22.54	22.53	22.84	22.91
Ti	0.01	0.01	0.01	0.01	0.00	0.01
Al	9.82	9.32	9.46	9.47	9.16	9.09
Cr	0.00	0.00	0.02	0.00	0.00	0.02
V	0.00	0.01	0.01	0.01	0.00	0.01
Fe^{3+}	0.00	0.00	0.02	0.00	0.00	0.02
Mn	0.00	0.05	0.02	0.01	0.05	0.02
Mg	0.03	0.02	0.02	0.07	0.01	0.04
Ca	2.03	1.01	1.23	1.36	0.19	0.48
Sr	0.00	0.00	0.01	0.00	0.00	0.01
Ba	0.01	0.00	0.02	0.00	0.01	0.02
Na	0.31	0.41	0.43	0.43	0.28	0.51
K	5.36	6.97	6.64	6.37	8.41	7.72
Ni	0.00	0.07	0.01	0.02	0.00	0.01
P	0.00	0.02	0.01	0.00	0.00	0.01
Total	39.75	40.56	40.44	40.28	40.95	40.88
H_2O	13.62	7.52	10.45	10.31	8.60	8.96
$Al+Fe^{3+}$	9.8	9.3	9.5	9.5	9.2	9.1
Al theor.	9.8	9.5	9.7	9.7	9.2	9.4
E	0.1	−2.2	−1.5	−2.0	−0.4	−2.5

the room-temperature structure of the 'true' phillipsite space group $P2_1/m$ (Gatta *et al*., 2009) and the phillipsite domain modelled in the present study, using a twinned merlinoite-like unit cell in space group $P12_1/m1$. In true phillipsite (Gatta *et al*., 2009), all adjacent eight-membered ring channels running parallel to *b* are identical by translation (Fig. 2). This is not so in our simplified model, in which directly adjacent channels are related only by a 2_1 operation along *b* and not by translation (Fig. 6, right column). However, at room temperature our approach provides a fair approximation of both structures.

https://doi.org/10.1180/minmag.2015.079.1.15 Published online by Cambridge University Press

Dehydration and framework distortion

The variation of the cell volume of the Monte Somma merlinoite/phillipsite intergrowth with temperature is displayed in Fig. 7. The development of cell volume with temperature is intermediate between those of merlinoite from the Khibiny massif, Russia (Pakhomova *et al*., 2014) and Ba-rich phillipsite (Sani *et al*., 2002). The framework of Monte Somma merlinoite at 250ºC refined with the $P12_1/m1$ model (Fig. 8*b*) is very similar to the completely dehydrated merlinoite (Fig. 8*a*, 225ºC, space group $P4_2/nmc$) from the Khibiny massif, Russia (Pakhomova *et al*., 2014). This indicates that upon dehydration the MER framework undergoes strong distortion, which may be described by rotation of the adjacent four-membered rings in the double crankshafts running along the *c* axis. Thus the eight-membered ring channels along *c* become strongly elliptically deformed (Fig. 8*a*) with the short and the long elliptical half axis alternately rotated 90º around *c*. This arrangement also leads to the formation of small apertures of square cross-section in projections down *c* (Fig. 8*a*). Thus, Monte Somma merlinoite shows a different high-temperature distortion compared to the synthetic sample $K_{11.5}[Al_{11.5}Si_{20.5}O_{64}]$ (Skofteland *et al*., 2001) but deforms in a similar style to the sample of Pakhomova *et al*. (2014).

The simplified $P12_1/m1$ approach fails to resolve a high-temperature structure model for phillipsite. This may be easily explained, as the difference between dehydrated merlinoite and phillipsite at high temperature (Fig. 8*a*,*c*) can no longer be modelled only by *b*/2 shifts of two tetrahedra. As shown in Fig. 8, the 'expected' high-temperature structures of merlinoite (Pakhomova *et al*., 2014) and phillipsite (Sani *et al*., 2002) show strong differences that are easily recognized by the distinct channel cross-sections.

Note that the first structural model for phillipsite (Steinfink, 1962) used a merlinoite-like unit cell of a = 9.96, b = 14.25, c = 14.25 Å with the orthorhombic space group $B2mb$. This choice of space group represents a geometric average of complex twinning of individuals of monoclinic $P2_1/m$ symmetry with a = 9.87, b = 14.30, c = 8.67 Å, β = 124.2º (Rinaldi *et al*., 1974). However, such a *B*-centred cell is not compatible with the framework of merlinoite and cannot be used for description of a merlinoite/phillipsite coherent intergrowth.

Temperature-dependent distortion in chabazite inclusions

Small chabazite inclusions were detected only as a subordinate phase in the diffraction pattern of one merlinoite/phillipsite intergrowth from Monte

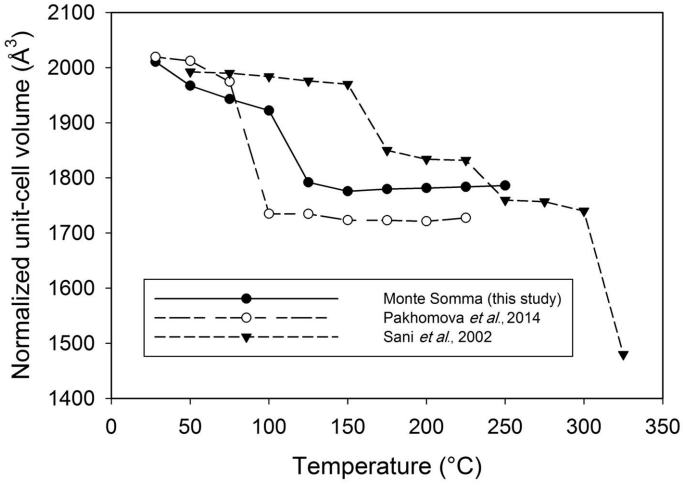

FIG. 7. Volume dependence of merlinoite $NaK_{11}[Al_{12}Si_{20}O_{64}]\cdot 15H_2O$ (Pakhomova *et al*., 2014), Monte Somma merlinoite/phillipsite (this study) and Ba-phillipsite (Sani *et al*., 2002) upon *in situ* dehydration. The Ba-phillipsite volume is doubled to be comparable with merlinoite. The size of the symbols is significantly larger than associated standard deviations.

https://doi.org/10.1180/minmag.2015.079.1.15 Published online by Cambridge University Press

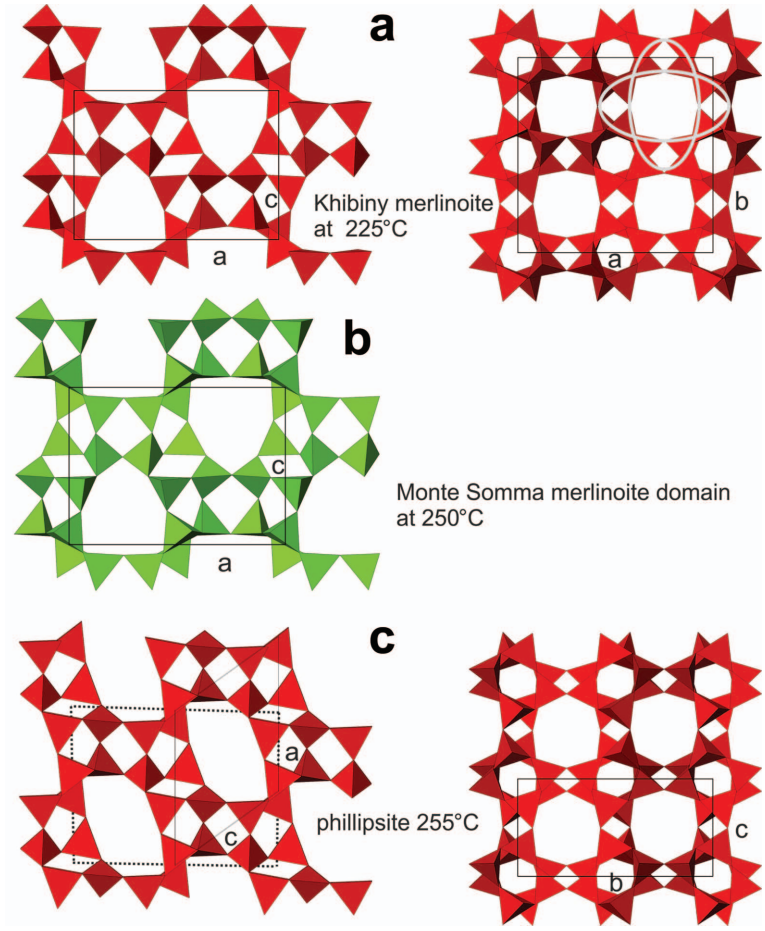

FIG. 8. (*a*) High-temperature distortion of the merlinoite framework for a sample from the Khibiny massif, Russia (Pakhomova *et al*., 2014). (*b*) Refined crystal structure of the merlinoite domain from Monte Somma at 250ºC (present study). A projection along the *c* axis (not displayed) is also identical to the corresponding representation of Khibiny merlinoite. (*c*) Phillipsite framework at 255ºC (Sani *et al*., 2002), dotted unit cell corresponds to the merlinoite cell. Solid lines represent the true unit-cell outlines.

Somma. Unfortunately, detailed electron-microprobe analyses of merlinoite-like crystals from the same sample failed to indicate the chemical composition of chabazite. As chabazite has a very similar Al/Si ratio to merlinoite and phillipsite and also similar extra-framework content, we cannot exclude the possibility that some analysed points with low K concentrations represent chabazite composition. Structural distortion upon dehydration of chabazite $Ca_{1.1}K_{0.7}Na_{0.4}[Al_{3.4}Si_{8.6}O_{24}]\cdot 14.4H_2O$ (Talisker Bay, Isle of Skye, Scotland) has been analysed thoroughly by Zema *et al*. (2008). Because detailed information on the extra-framework composition of this Monte Somma chabazite is lacking, here we discuss only the important aspects of its behaviour upon dehydration. Our results also emphasize how powerful area detectors are for the investigation of composite mineral aggregates by single-crystal XRD.

Monte Somma chabazite (space group $R\bar{3}m$) at room temperature a = 13.836(3), c = 15.001(4) Å, V = 2486.9(6) Å^3 shows only small (3%) volume contraction (Fig. 9) upon dehydration up to 250ºC: a = 13.4275(19), c = 15.510(3) Å, V = 2421.7(8) Å^3. The unit-cell volume is kept nearly constant because while the a parameter decreases, the c parameter increases (Fig. 9). This behaviour

https://doi.org/10.1180/minmag.2015.079.1.15 Published online by Cambridge University Press

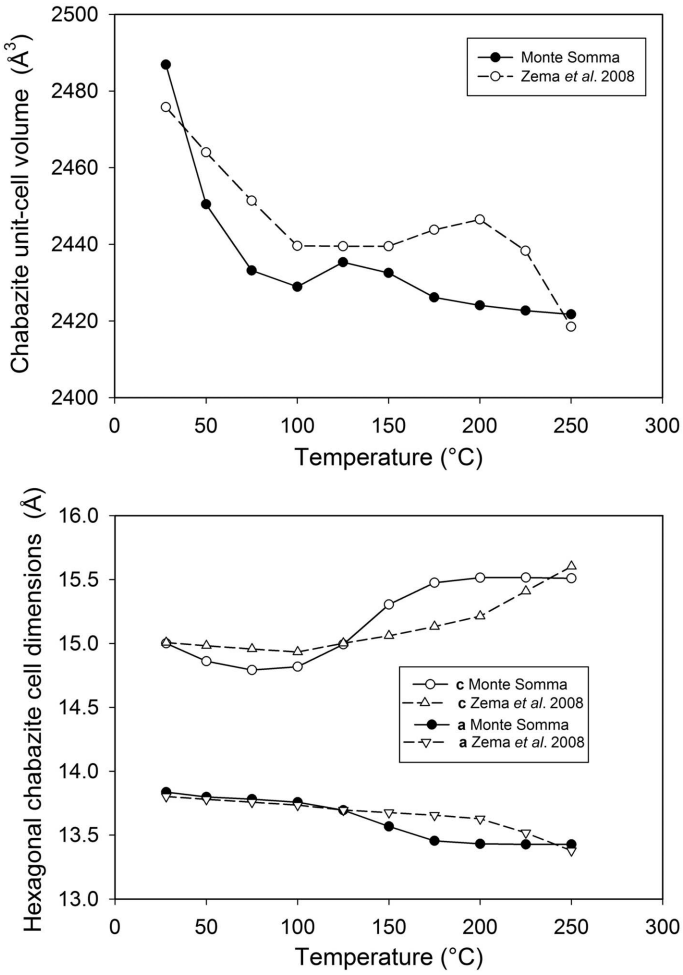

FIG. 9. Temperature dependence of unit-cell dimensions of chabazite from Monte Somma (present study) and from the Isle of Skye (Zema *et al*., 2008). The size of the symbols is significantly larger than associated standard deviations.

is consistent qualitatively with the data of Zema *et al*. (2008). In our sample the main distortional effect in the framework occurs between 125 and 150ºC, when the six-membered rings forming the double-ring units distort and twist strongly (Fig. 10). This also affects the eight-membered rings between the double-ring units, which change from originally rounded to strongly elongated parallel to *c*. The corresponding distortion in the chabazite from Skye (Zema *et al*., 2008) starts at ~200ºC and is accompanied by a volume maximum in Fig. 9.

Without knowing the chemical composition of the Monte Somma chabazite, and considering the weak intensity of X-ray reflections of the subordinate chabazite phase, the interpretations of extra-framework occupants have only a semi-quantitative character. At 50ºC the major cation site *C*2 (Zema *et al*., 2008) crowns on the six-membered ring of tetrahedra, while the opposite side is shielded by H_2O. Note that this site was split into *K*1, *K*2 and *Na*2 subsites by Yakubovich *et al*. (2005). The centres of eight-membered rings are plugged by the low-occupancy *C*5 site (labelled according to Zema *et al*., 2008). At 125ºC, the main part of H_2O coordinating *C*2 is released and *C*2 moves closer to the centre of a six-membered ring; the occupancy of *C*5

https://doi.org/10.1180/minmag.2015.079.1.15 Published online by Cambridge University Press

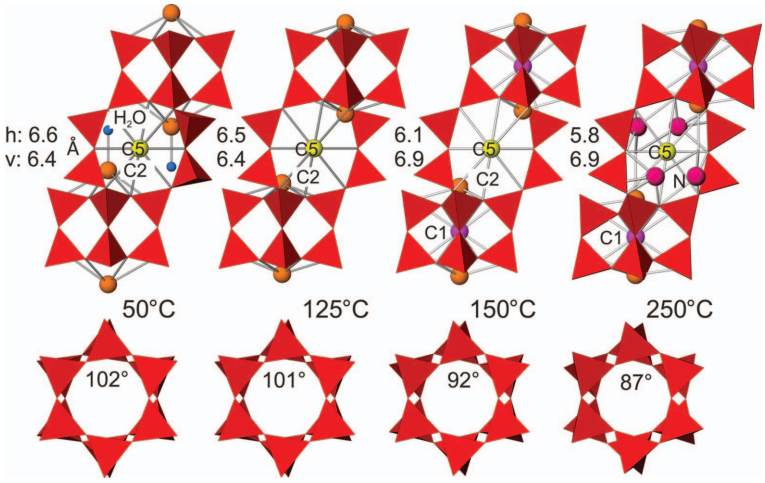

FIG. 10. Temperature dependence of the chabazite structure of the Monte Somma sample; upper row: projected parallel to *a*, with the *c* axis vertical. Dimensions of the eight-membered ring of tetrahedra are given in h = horizontal and v = vertical directions. Prominent extra-framework sites are labelled. Lower row: six-membered double-ring units are projected parallel to *c*. The decrease of the more acute O–O–O angle with temperature associated with increased twisting of the six-membered rings is shown.

increases. At 150ºC, accompanied by distortion of the six-membered rings, the occupancy at *C*2 decreases and the new site, *C*1, occurs in the centre of the double-ring units. At 250ºC the occupancy at *C*5 decreases further and a new site (*N*) forms that is bonded to the cavity walls (Fig. 10).

Previous studies on phillipsite/merlinoite intergrowth

Even before the discovery of merlinoite in nature, its structure was generated along with that of phillipsite by Smith and Rinaldi (1962) and Smith (1968), who derived theoretical framework structures formed from parallel four- and eight-membered rings. The merlinoite and phillipsite structures are two of the 17 double crankshaft structures that they defined with UUDD (U: apex up; D: apex down) orientations of tetrahedra within the four-membered rings.

Passaglia *et al*. (1977), introducing merlinoite as new mineral from Cupaello, Rieti (Italy), emphasized the morphological differences between phillipsite and merlinoite at this locality. They noted that unequivocal distinction between merlinoite and phillipsite is possible only by XRD. Although the two powder diffraction patterns are similar, the diffraction peaks at d = 10.02 and 4.475 Å occur in merlinoite but are absent in phillipsite. In contrast, the line at d = 6.4 Å (medium intensity in phillipsite) is absent in merlinoite. Galli *et al*. (1979) solved the merlinoite structure and underscored the close structural relationship to phillipsite.

Sato and Gottardi (1982) investigated the slipping schemes that inter-relate double crankshaft tectosilicate structures and deduced the following implications for MER and PHI framework types: (1) slipping transformations from PHI to MER frameworks are likely to exist; (2) an overgrowth of PHI and MER frameworks exist (unfortunately, only personal communications from G. Hentschel and E. Franco were cited); and (3) stacking faults according to a slipping scheme that interconverts PHI and MER frameworks may occur in those structure types.

Russo and Preite (2011) cite powder XRD investigations on alleged merlinoite from Monte Somma by D. Gatta and N. Rotiroti, who interpreted supposed macroscopic single crystals of merlinoite to be composed of an intergrowth of both merlinoite and phillipsite. The present study confirms this interpretation and demonstrates the coherent intergrowth of both frameworks on a submicroscopic scale. The actual size of these domains remains an open question for further study.

https://doi.org/10.1180/minmag.2015.079.1.15 Published online by Cambridge University Press

Acknowledgements

The authors thank Giancarlo Della Ventura for providing a merlinoite/phillipsite sample from Fosso Atici. The constructive comments of Pete Leverett and three anonymous reviewers are much appreciated.

References

Bieniok, A., Bornholdt, K., Brendel, U. and Baur, W.H. (1996) Synthesis and crystal structure of zeolite W, resembling the mineral merlinoite. *Journal of Materials Chemistry*, **6**, 271–275.

Bruker (1999) *SMART and SAINT-PLUS, Version 6.01 (1999)*. Bruker AXS Inc., Madison, Wisconsin, USA.

Della Ventura, G., Parodi, G.C. and Burragato, F. (1993) New data on merlinoite and related zeolites. *Rendiconti Lincei Scienze Fisiche e Naturali*, **Ser**. **9(4)**, 303–312.

Galli, E., Gottardi, G. and Pongiluppi, D. (1979) The crystal structure of the zeolite merlinoite. *Neues Jahrbuch für Mineralogie, Monatshefte*, **1979**, 1–9.

Gatta, G.D., Cappelletti, P., Rotiroti, N., Slebodnik, C. and Rinaldi, R. (2009) New insights into the crystal structure and crystal chemistry of the zeolite phillipsite. *American Mineralogist*, **94**, 190–199.

Pakhomova, A.S., Armbruster, T., Krivovichev, S.V. and Yakovenchuk, V.N. (2014) Dehydration of the zeolite merlinoite from the Khibiny massif, Russia: an in situ temperature-dependent single-crystal X-ray study. *European Journal of Mineralogy*, **26**, 371–380.

Passaglia, E., Pongiluppi, D. and Rinaldi, R. (1977) Merlinoite, a new mineral of the zeolite group. *Neues Jahrbuch für Mineralogie, Monatshefte*, **1977**, 355–364.

Rinaldi, R., Pluth, J.J. and Smith, J.V. (1974) Zeolites of the phillipsite family. Refinement of the crystal structures of phillipsite and harmotome. *Acta Crystallographica*, **B30**, 2426–2433.

Russo, M. and Preite, D. (2011) Merlinoite del Monte Somma. *MICRO: Periodico dell'Associazione Micromineralogica Italiana*, **2/2011**, 64–65.

Sani, A., Cruciani, G. and Gualtieri, A.F. (2002) Dehydration dynamics of Ba-phillipsite: An in situ synchrotron powder diffraction study. *Physics and Chemistry of Minerals*, **29**, 351–361.

Sato, M. and Gottardi, G. (1982) The slipping scheme of the double crankshaft structures in tectosilicates and its mineralogical implication. *Zeitschrift für Kristallographie*, **161**, 187–194.

Sheldrick, G.M. (2008) A short history of *SHELX*. *Acta Crystallographica*, **A64**, 112–122.

Sherman, J.D. (1977) Identification and characterization of zeolites synthesized in the K_2O–$A1_2O_3$–SiO_2–H_2O system: Pp. 30–42 in: *Molecular Sieves II* (J.R. Katzer, editor). Symposium Series **40**, American Chemical Society, Washington, DC.

Skofteland, B.M., Ellestad, O.H. and Lillerud, K.P. (2001) Potassium merlinoite: crystallization, structural and thermal properties. *Microporous Mesoporous Materials*, **43**, 61–71.

Smith, J.V. (1968) Further discussion of framework structures built from four- and eight-membered rings. *Mineralogical Magazine*, **38**, 640–642.

Smith, J.V. and Rinaldi, F. (1962) Framework structures from parallel four- and eight-membered rings. *Mineralogical Magazine*, **32**, 202–212.

Steinfink, H. (1962) The crystal structure of the zeolite, phillipsite. *Acta Crystallographica*, **15**, 644–651.

Tschernich, R.W. (1992) *Zeolites of the World*. Geoscience Press, Phoenix, Arizona, USA, 563 pp.

Yakubovich, O.V., Massa, W., Gavrilenko, P.G. and Pekov, I.V. (2005) Crystal structure of chabazite K. *Crystallography Reports*, **50**, 544–553

Zema, M., Tarantino, S.C. and Montagna, G. (2008) Hydration/dehydration and cation migration processes at high temperature in zeolite chabazite. *Chemistry of Materials*, **20**, 5876–5887.

https://doi.org/10.1180/minmag.2015.079.1.15 Published online by Cambridge University Press